Onset and Evolution of $m/n = 2/1$ Neoclassical Tearing Modes in High-β_p Mode Discharges in JT-60U

Akihiko ISAYAMA, Go MATSUNAGA, Yoichi HIRANO[1)] and the JT-60 Team

Japan Atomic Energy Agency, Naka, Ibaraki 311-0193, Japan
[1)]*Nihon University, 1-8-14 Kanda-Surugadai, Chiyoda-ku, Tokyo 101-8308, Japan*

(Received 2 October 2012 / Accepted 27 December 2012)

The onset and evolution of an $m/n = 2/1$ neoclassical tearing mode (NTM) in JT-60U under nearly constant discharge conditions are investigated (m and n are the poloidal and toroidal mode numbers, respectively.). In about 80% of the discharges, the 2/1 NTM appears from a small amplitude without a noticeable triggering event, and in the rest of the discharges, the 2/1 NTM is triggered by a collapse localized at the mode location. Although the former grows with regular oscillations of the magnetic perturbations, the latter grows with irregular oscillations from the beginning. In addition, although a collapse causing a temperature change of ~20% triggers a 2/1 NTM, a smaller-amplitude collapse, e.g., a temperature change of ~7%, does not trigger an NTM. This suggests the existence of a threshold amplitude that triggers an NTM. The characteristics of the localized collapse are similar to those of a previously observed barrier localized mode.

Keywords: neoclassical tearing mode, instability, JT-60U, tokamak

DOI: 10.1585/pfr.8.1402013

1. Introduction

In a fusion reactor, a high-pressure plasma needs to be sustained in the steady state. It is known that a neoclassical tearing mode (NTM), which is one of the magnetohydrodynamic (MHD) instabilities, appears in a high-pressure tokamak plasma with a positive magnetic shear [1]. Because NTMs degrade the plasma pressure and sometimes cause a disruption, understanding the physics of NTMs and establishing methods for controlling them are important. In particular, NTMs with $m/n = 3/2$ and $2/1$ are important because their effect on plasma confinement is large. Here m and n are the poloidal and toroidal mode numbers, respectively.

Electron cyclotron current drive (ECCD) is considered to be the most promising method of controlling NTMs, and its effectiveness was demonstrated in ASDEX-U [2–4], DIII-D [5–7], and JT-60U [8–11]. A real-time system for NTM control was developed to a highly sophisticated level, and experiments using these systems were also conducted. For example, in JT-60U, real-time optimization of the injection angle of electron cyclotron (EC) waves [9] and real-time setting of the pulse duration and injection timing for modulated ECCD [11] were demonstrated.

On the other hand, regarding NTM physics, although it was demonstrated that the behavior of NTMs with a large amplitude is well fitted with the modified Rutherford equation [12–14], their behavior at a small amplitude, especially near their onset, is still under investigation because of their complex mechanism consisting of many competing effects [15]. In addition, from the viewpoint of experimental research, the measurement of magnetic islands in the very early phase of NTM growth is difficult because of the limited spatial resolution and signal-to-noise ratio of diagnostic systems. It was observed previously that NTMs are triggered by other instabilities such as sawtooth oscillations, fishbone instabilities, and edge localized modes (ELMs) [16, 17]. It was also observed that, as in JT-60U, NTMs can appear without such instabilities [18]. Thus, the clarification of NTM physics, especially at mode onset, is a profound topic. However, even aside from the details of the physics of NTM onset, it is important to clarify the characteristics of the onset and growth of NTMs and prepare a real-time system for NTM control according to their behavior.

This paper describes the onset and evolution of an $m/n = 2/1$ NTM in JT-60U. The analysis used a data set of experiments on the stabilization of $m/n = 2/1$ NTMs [10, 11] in which the plasma parameters were almost the same to obtain a similar 2/1 NTM for inter-shot comparison of ECCD effects. Statistical analysis will make it possible to reveal how much, if at all, the onset and growth of the 2/1 NTM varies. In addition, because the high-β_p mode analyzed in this paper is similar to the Hybrid Scenario in ITER [19], it is expected that the results can contribute to defining the requirement for NTM stabilization in ITER, which is now under consideration by the ITER team.

The structure of this paper is as follows. Section 2 describes the conditions of the NTM experiments. The results of the analysis are presented in Sec. 3. The onset

author's e-mail: isayama.akihiko@jaea.go.jp

regime of the 2/1 mode, types of mode onset and growth, and effects of profiles on mode onset are described. Finally, a summary and discussion are presented in Sec. 4.

2. Experimental Setup

In this series of NTM experiments, the discharge conditions such as the plasma shape and heating scheme were nearly constant, so that an $m/n = 2/1$ mode was reliably obtained. An example of a high-β_p mode discharge is shown in Fig. 1. The typical plasma parameters are as follows: the plasma current $I_p = 1.5$ MA, toroidal magnetic field at the plasma geometric center $B_t = 3.7$ T, major radius $R = 3.23$ m, minor radius $a = 0.78$ m, and safety factor at 95% flux surface $q_{95} = 4.0$. Neutral beams (NBs) with a total power of 22 MW were injected at $t = 4.8$ s to raise the plasma pressure. Although the NBs were injected with preprogrammed waveforms in most of the discharges, the injection power was controlled by feedback in some discharges, as shown later in Fig. 12. The values of the normalized beta, $\beta_N = \beta/(I_p/aB_t)$, and the poloidal beta, β_p, reached ~2 and ~1.5, respectively, at $t = 5.63$ s.

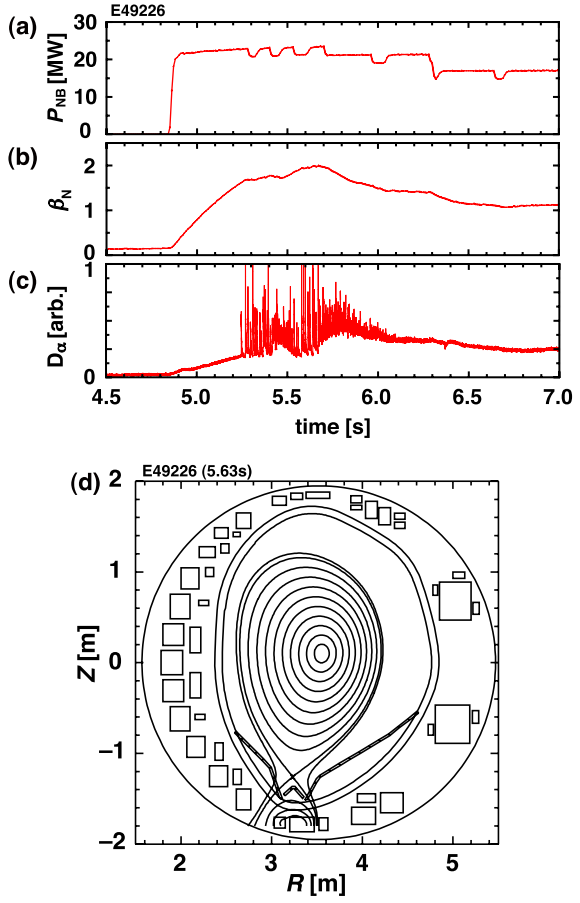

Fig. 1 Typical discharge of an NTM experiment. (a) Neutral beam power, (b) normalized beta, (c) D_α intensity, and (d) plasma cross section. The degradation of the stored energy at t 5.7 s is caused by a 2/1 NTM.

Here β is the ratio of the plasma pressure to magnetic pressure. The line-averaged electron density $\bar{n}_e$ and central ion temperature T_i are typically 3×10^{19} m^{-3} and 15 keV, respectively. Here the sight line of the line-averaged electron density is in the vertical direction at $R = 3.55$ m, which is close to the magnetic axis location in a high-β phase. The plasma enters a high-confinement mode with ELMs at $t \approx 5.25$ s. Each ELM is observed as a spike in the D_α intensity signals and magnetic perturbation signals, as shown later (e.g., Figs. 3 (a) and (b)).

The injection time of NBs was set so as to keep the central safety factor, $q(0)$, slightly above unity; the value of $q(0)$ decreases below unity and sawtooth oscillations appear if the injection time is too late. In fact, no sawtooth oscillation was observed in this phase. The NB injection power was adjusted slightly to obtain an $m/n = 2/1$ mode reproducibly; an $m/n = 3/2$ mode appears when the beta value is lower than that for the onset of a 2/1 NTM, and no mode appears when the power is even lower. Typical locations of an $m/n = 3/2$ and 2/1 mode are $\rho = 0.4$ and 0.5, respectively, where ρ is the volume-averaged normalized minor radius. Because mode onset is determined by the pressure and current profiles, the injection power was adjusted by investigating the mode behavior and the temperature, density, and current density profiles.

After the appearance of an $m/n = 2/1$ NTM at $t = 5.5$–6.5 s, the β_N value decreased by about 30% (a 2/1 mode appeared at $t = 5.635$ s in shot E49226, shown in Fig. 1). Soon after the onset and growth of the 2/1 mode, the mode frequency, which is roughly proportional to the toroidal rotation velocity [20], slowed down and stayed at ~300 Hz owing to the growth of magnetic islands, as shown in the next section.

3. Analysis

3.1 Characterization of mode onset

The analyzed data set consists of about 40 discharges in NTM stabilization experiments. The onset and evolution were first analyzed using magnetic probe signals because of their high signal-to-noise ratio. The structure of the 2/1 mode was analyzed by using electron cyclotron emission (ECE) diagnostics, which consists of a 12-channel heterodyne radiometer with a channel separation of ~2 cm and a 20-channel grating polychromator with a channel separation of ~6 cm. The former was used for measurement in the region around magnetic islands, and the latter was used to measure the global temperature evolution. The sight line of the ECE diagnostics is in the horizontal direction at +0.2 m above the center of the vacuum vessel ($Z = 0.2$ m in Fig. 1 (d)).

The value of β_N at mode onset is plotted against the onset time in Fig. 2. If the value of β_N exceeds about 2, the discharge was terminated by a beta collapse. In such cases, no NTM was observed. When the β_N value was kept at about 2 for, typically, several hundred millisec-

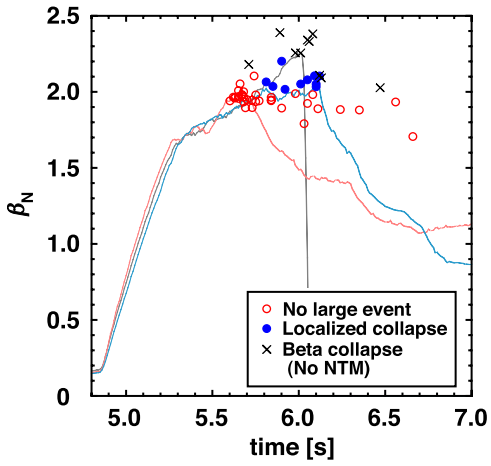

Fig. 2 Normalized beta at mode onset or beta collapse. The open circles correspond to mode onset growing from a small amplitude, and the closed circles correspond to mode onset triggered by a localized collapse. The cross symbols correspond to discharges terminated by a beta collapse, in which no NTM was observed. The time traces of the normalized beta for typical discharges are also shown.

onds, an $m/n = 2/1$ NTM appeared. Among the discharges in which a 2/1 mode appeared, the onset behavior can be classified into two groups according to the waveform of the magnetic perturbations and the electron temperature: (a) mode onset and growth from a small mode amplitude and (b) mode onset triggered by a localized collapse. Moreover, the former constitutes about 80% of the analyzed discharges, and the latter accounts for about 20%. The appearance time of the former covers a wide range: $t = 5.6$–6.7 s; in particular, mode onset at $t \sim 5.7$ s is most frequently observed. The latter seems to appear in a slightly higher-beta region and at a later time.

3.2 Characteristics of mode behavior

3.2.1 Mode onset and growth from a small mode amplitude

The temporal evolution of magnetic perturbations that appear without a large MHD event is shown in Fig. 3. In this case, the mode amplitude increases from nearly the noise level and saturates in ~50 ms. As the mode grows, the mode frequency decreases starting at $t \approx 5.68$ s and reaches ~400 s^{-1}. In Fig. 3 (a), the temporal evolution of the D_α intensity is shown. The spikes at, for example, $t = 5.614$, 5.624, and 5.641 s correspond to perturbations by ELMs. The fact that the mode starts to grow between ELMs suggests that the 2/1 mode was not triggered by an ELM. The temporal evolution of the electron temperature around the mode location measured with a heterodyne radiometer is shown in Fig. 3 (c). Oscillations first appear at channels 2–4, which correspond to $\rho \approx 0.5$. An inversion of the phase of the oscillations, which is an indication of

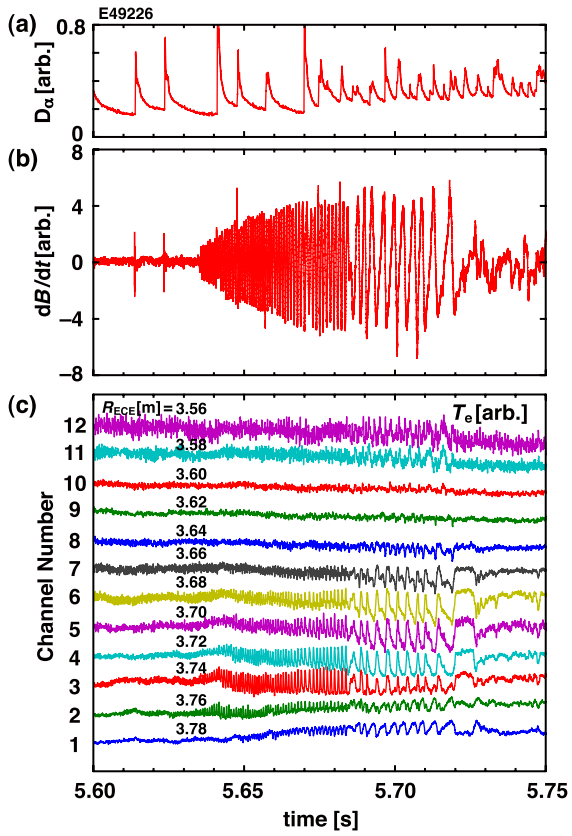

Fig. 3 Expanded view of shot E49226 near mode onset. (a) D_α intensity, (b) magnetic perturbation amplitude, and (c) electron temperature measured with a heterodyne radiometer. R_{ECE} is the measurement point of each channel.

magnetic island formation, can also be seen across channels 1–4. The full width of the magnetic islands at mode saturation is typically 10–15 cm. After $t = 5.72$ s, the oscillations of the magnetic perturbation signal become unclear because the mode frequency becomes very low. The existence of a magnetic island can be confirmed from the ECE signals: the signal of channel 1 stays at the lower level of the oscillations, whereas the signals of channels 5–7 stay at the higher level. This feature indicates that the measurement points of the heterodyne radiometer correspond to the X-point of the magnetic island.

Figure 4 shows a plot of $1/\Delta t_{peak}$ against $(dB/dt|_{t=t_{peak}})/(1/\Delta t_{peak})$. Here t_{peak} is the time at which dB/dt reaches a local maximum, Δt_{peak} is the time difference between two successive peaks, and $dB/dt|_{t=t_{peak}}$ is the value of dB/dt at the local maximum. Thus, $1/\Delta t_{peak}$ corresponds to the mode frequency, and $(dB/dt|_{t=t_{peak}})/(1/\Delta t_{peak})$ corresponds to the time derivative of the mode amplitude normalized to the mode frequency, or equivalently, the mode amplitude. The mode frequency decreases from 1300 Hz with increasing mode amplitude and reaches ~700 Hz; then, it decreases rapidly to 400 Hz with increasing mode amplitude. This behavior is similar to that in previous observations, where the mode frequency suddenly decreased from

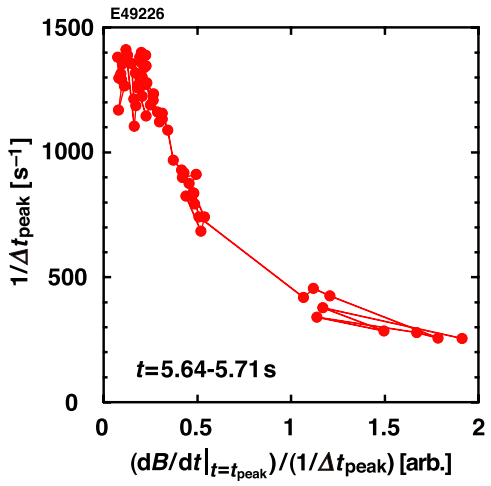

Fig. 4 Relationship between $dB/dt|_{t=t_{peak}}/(1/\Delta t_{peak})$ and $1/\Delta t_{peak}$, where $dB/dt|_{t=t_{peak}}$ and $1/\Delta t_{peak}$ correspond to the peak value of the magnetic perturbation amplitude and inverse of time difference between two successive peaks, respectively. The horizontal and vertical axes correspond to the mode amplitude and mode frequency, respectively.

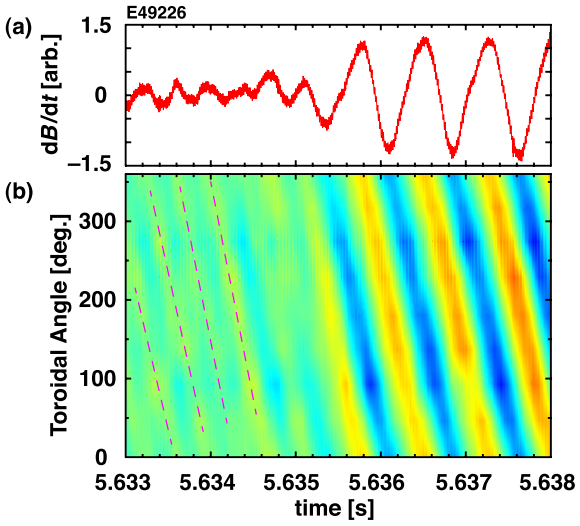

Fig. 5 Magnetic perturbations at the onset of an $m/n = 2/1$ mode in shot E49226. (a) Temporal evolution at the toroidal angle and (b) temporal evolution of toroidal structure. In (b), dotted lines are added to guide the eye.

~2.5 kHz to ~0.5 kHz when the width of the NTM islands was increased by misaligned ECCD [20].

The temporal evolution of the magnetic perturbations at mode onset is shown in Fig. 5. The oscillations after $t = 5.635$ s having an $n = 1$ structure correspond to an $m/n = 2/1$ mode. Before mode onset, weak oscillations are observed. The oscillations have an $n = 2$ structure, as shown in this figure. The frequency spectrum of the ECE signals indicates that the amplitude of the $n = 2$ oscillations is largest at channels 6 and 7, which correspond to the inner side (nearer to the plasma center) of the phase inversion location of the $n = 1$ oscillations (channel 2). In addition, a phase inversion is observed across channels 8–10. Thus, the $n = 2$ oscillations correspond to an $m/n = 3/2$ mode. Although the mode locations differ (~14 cm apart), the toroidal structure appears to connect smoothly owing to a similar rotational velocity at these locations: the peak of the magnetic perturbation amplitude in Fig. 5 (b) propagates at a similar speed.

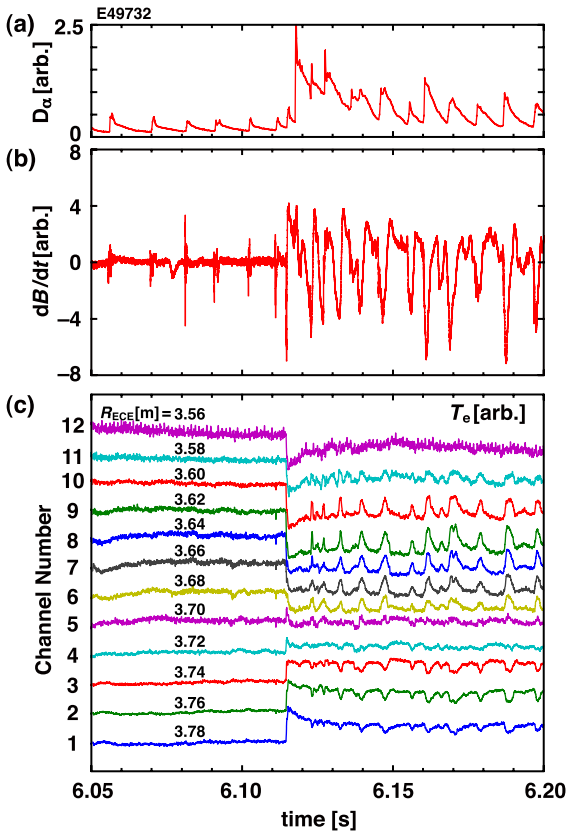

Fig. 6 Typical discharge with an NTM triggered by a localized collapse. (a) D_α intensity, (b) magnetic perturbation amplitude, and (c) electron temperature measured with a heterodyne radiometer.

3.2.2 Mode onset triggered by a localized collapse

In around 20% of the analyzed shots, large magnetic perturbations appeared suddenly with a large amplitude from the beginning. Analysis using ECE diagnostics revealed that this type of onset is caused by a small collapse localized at the mode location. The temporal evolution of the magnetic perturbations and electron temperature are shown in Fig. 6. A collapse occurs at $t = 6.114$ s, and irregular oscillations appear just after the collapse. In fact, such irregular oscillations, a phase inversion across channels 4–6, which is the same result as the previous example, can be recognized. The location where the change in the electron temperature at the collapse is smallest, which corresponds to the location of the collapse, is also located at this po-

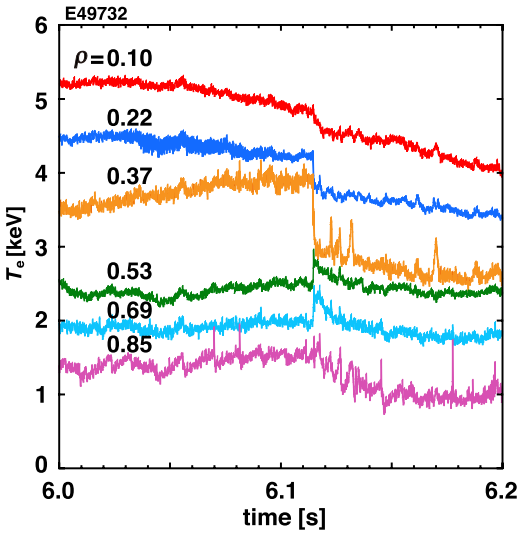

Fig. 7 Time evolution of electron temperature measured with a grating polychromator in shot E49732. Rapid changes in electron temperature observed only at $\rho = 0.85$ correspond to ELMs.

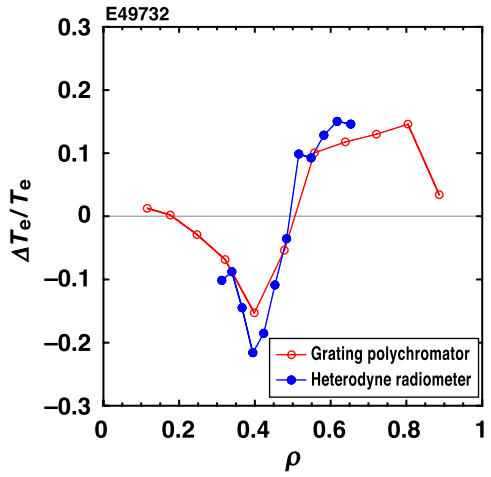

Fig. 8 Profiles of temperature differences during a localized collapse. The open and closed circles correspond to profiles measured with a grating polychromator and heterodyne radiometer, respectively.

sition. Thus, the collapse is also localized at the $q = 2$ surface.

Figure 7 shows the evolution of the electron temperature from the center to edge measured with a grating polychromator. Although the central electron temperature decreases after the collapse, the change rate is much slower than that at the $q = 2$ surface. In addition, the change in the edge region is small (rapid decreases observed in the edge channel correspond to ELM crashes). Figure 8 shows the profiles of the change rate of the electron temperature at the collapse evaluated from the signals of a grating polychromator and heterodyne radiometer. Although the profiles

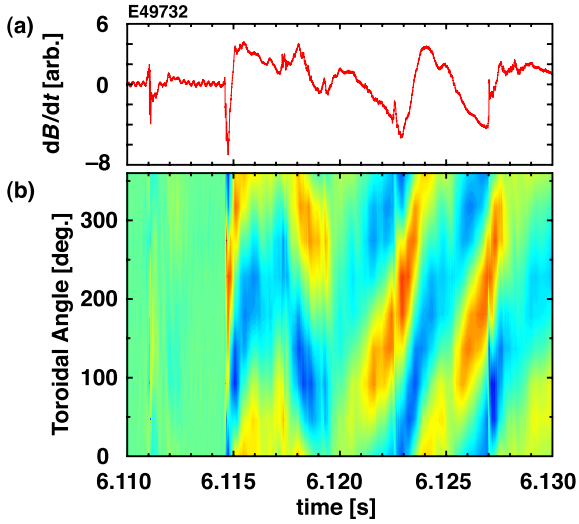

Fig. 9 Magnetic perturbations at the onset of an $m/n = 2/1$ mode in shot E49732. (a) Temporal evolution at the toroidal angle and (b) temporal evolution of toroidal structure.

differ slightly due to the difference in the spatial resolution of each diagnostic, a similar localization of the change rate at $\rho \approx 0.5$ is found. The change rate reaches approximately $\pm 15\%$ near the mode location, and it decreases to $\sim 5\%$ at $\rho \approx 0.3$. Near the plasma center, it is almost zero.

The temporal evolution of the magnetic perturbations at mode onset is shown in Fig. 9. No large structure is seen before the localized collapse at $t = 6.115$ s. Just after the collapse an $n = 1$ structure is observed. The structure appears to rotate in the co-direction, i.e., the same direction as the plasma current, until $t \approx 6.117$ s, but then the rotation direction appears to reverse until $t \approx 6.120$ s. The rotation direction then reverses again at $t \approx 6.120$ s and the direction is maintained. This type of evolution is seen in other discharges with a localized collapse, and a variety of such apparent changes in the rotation direction is observed. A possible reason for the rotation change is the change in the measurement point at the collapse. Because the rotation profile is nearly zero owing to balanced NB injection, a slight change in the measurement points at a collapse can cause such an apparent rotation reversal.

An expanded view of the evolution of electron temperature around the localized collapse is shown in Fig. 10 (a). After the collapse, a fast change in the electron temperature, whose time scale is less than 1 ms, is seen in channels 1–10. The first temperature oscillation is seen at $t = 6.123$ s, which is about 8 ms after the collapse. The oscillation is observed in a wide region, channels 1–11. Figure 10 (b) shows the profile of the temperature difference at the oscillation at $t = 6.123$ s. The local maximum is located at $\rho \approx 0.40$ and the point crossing the zero amplitude is located at $\rho \approx 0.54$. In Fig. 10 (b), an amplitude profile at $t \approx 5.70$ s in shot E49226, at which time regular oscilla-

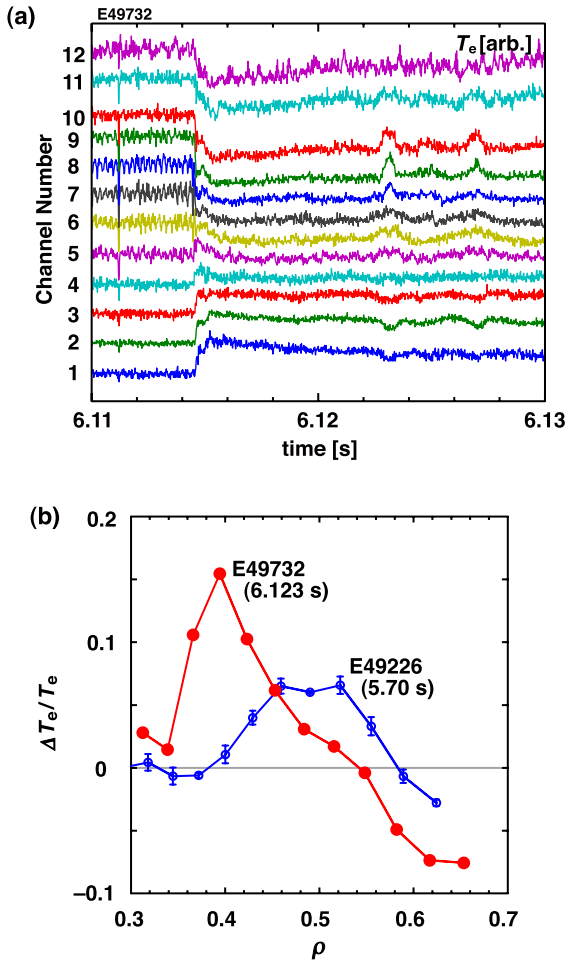

Fig. 10 (a) Electron temperature evolutions before and after a localized collapse and (b) profiles of the changes in the electron temperature at the oscillations at $t \approx 6.123$ s in shot E49732 and $t \approx 5.70$ s in shot E49226.

tions almost slowed down (see Fig. 3 for the temporal evolution), is also plotted. The profile was obtained from six periods with similar mode amplitudes. The profile shows that the location crossing the zero amplitude is located at $\rho \approx 0.58$ and the peak amplitude is located at $\rho \approx 0.48$, which indicates that the width of the inner half of the magnetic island is ~0.1 in ρ. Compared with this result, both the amplitude and width in shot E49732 are much larger than those in E49226 despite only ~10 ms after the localized collapse, which suggests that larger magnetic islands were formed in shot E49732.

The onset and evolution of the 2/1 mode after a localized collapse depends on the amplitude of the collapse. Figure 11 shows an example having a different behavior than that in shot E49732. In shot E46342, two small collapses appear at $t = 6.005$ s and 6.054 s, but a 2/1 mode is not triggered, and no magnetic perturbations owing to the collapses are observed. The value of $\Delta T_e/T_e$ at channel 9 ($\rho \approx 0.4$) is −7% for the collapse at $t = 6.054$ s. On the other hand, a 2/1 mode is triggered by a collapse with a

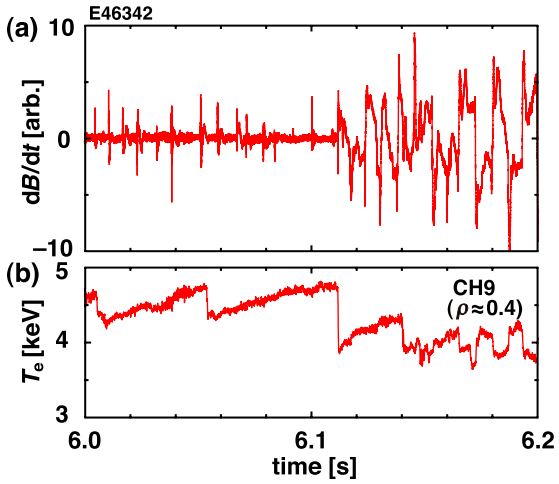

Fig. 11 Typical discharge with successive localized collapses. Localized collapses at $t = 6.005$ s and 6.054 s with a smaller amplitude do not trigger a 2/1 mode, whereas a collapse at $t = 6.112$ s triggers a 2/1 mode.

larger amplitude at $t = 6.112$ s. The value of $\Delta T_e/T_e$ at $\rho \approx 0.4$ is −18%, which is comparable to that in shot E49732 (Fig. 8). These results indicates that there is a threshold amplitude for triggering a 2/1 mode, whose value lies at $\Delta T_e/T_e = 7\%$–18% in this case.

3.3 Effect of profiles on mode behavior

As shown in Fig. 2, the beta value at which a localized collapse occurs is similar to the one at which a 2/1 NTM appears without such a collapse. This suggests that parameters other than the beta value contribute to the onset of the collapse. To investigate the difference in profiles, which is the most possible candidate, two similar discharges are compared in Fig. 12; a slowly growing NTM appeared at $t = 6.060$ s in shot E49736, and a collapse-induced NTM appeared at $t = 6.114$ s in shot E49732. As shown in the previous section, the plasma parameters such as I_p and B_t are the same in these discharges. In addition, the preprogrammed waveforms are the same. The beta value was controlled by feedback on the NB power, which causes a difference in the injection power. In fact, the averaged injection power at $t = 5.8$–6.1 s in shot E49732 is higher than that in shot E49736 by about ~15%. In these discharges, the evolution of the beta value is almost the same because of the feedback control. The line-averaged electron density in shot E49732, which was controlled by feedback until the NB injection, is higher than that in shot E49736 by ~5%, and no deuterium gas puff was done during the NB phase in these discharges. Furthermore, the base level of the D_α intensity in shot E49732 is higher than that in shot E49736 by ~30%. The differences during the NB phase are possibly due to some changes in the wall condition; this type of difference is often observed when the plasma configuration of the previous discharge, especially the location of the di-

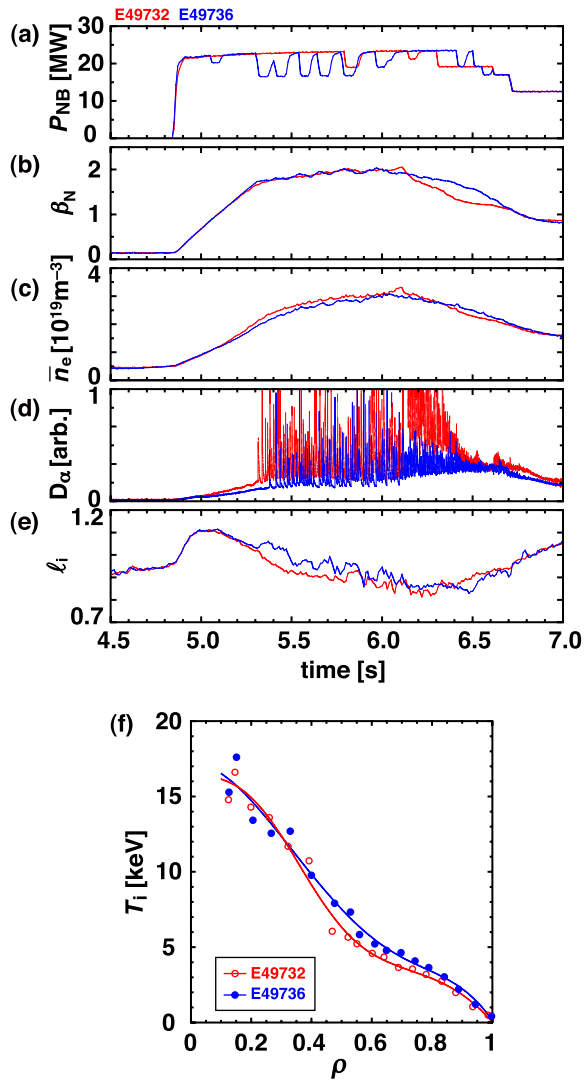

Fig. 12 Comparison of discharges with and without a localized collapse. (a) Neutral beam power, (b) normalized beta, (c) line-averaged electron density, (d) D_α intensity, and (e) internal inductance from equilibrium calculations assuming $q(0) = 1$ and (f) ion temperature profiles.

vertor legs, is different, which is the case in shot E49732. The evolution of the internal inductance ℓ_i evaluated from an equilibrium calculation assuming $q(0) = 1$ is shown in Fig. 12 (e). Although the value of ℓ_i at $t = 5.3$–6.0 s in shot E49736 is slightly higher than that in shot E49732, it is almost the same at mode onset. This suggests that the current profiles are similar at mode onset. Ion temperature profiles just before mode onset are shown in Fig. 12 (f). The temperature gradient at the mode location, $\rho \approx 0.5$, is steeper for shot E49732 because T_i in the central region is similar, whereas T_i in the peripheral region is lower in shot E49732. In addition, as can be seen in Fig. 7, a temperature difference between $\rho = 0.37$ and 0.57 gradually increases before the localized collapse. This difference in the pressure gradient at the mode location is considered to be the most probable reason for the difference in the onset behavior.

4. Discussion and Summary

The onset and evolution of an $m/n = 2/1$ NTM in high-β_p mode discharges in JT-60U were investigated. In about 80% of the analyzed data set, the mode grows gradually with regular oscillations. In the other 20%, the mode was triggered by a collapse at the $q = 2$ surface. In most such cases, the oscillations were irregular from the beginning. Moreover, no NTM is triggered when the change in the electron temperature is small (typically ~7%), and regular oscillations can also appear. This type of trigger event has not been reported before although NTMs triggered by a sawtooth crash or a fishbone instability were reported earlier [16, 17].

A localized collapse in a region of an internal transport barrier in high-β_p mode discharges was previously observed and termed the barrier localized mode (BLM) [21]. The behavior of the collapse in this paper is similar to the BLM: (a) localization at the $q = 2$ surface where a steep pressure gradient is formed, (b) appearance at high-beta values ~10%–20% lower than the values at which a beta collapse occurs, (c) time scale in the order of microseconds, and (d) occurrence at a high pressure gradient at the mode location. In the discharge shown in Ref. [21], no NTM was triggered. This may be attributed to a smaller mode amplitude ($\Delta T_e/T_e \approx 10\%$) or lower bootstrap current density at the $q = 2$ surface located in a more peripheral region.

When an NTM is stabilized by modulated ECCD, the frequency and phase of the NTM need to be identified to determine the pulse duration and trigger time, respectively, of the injected EC waves. In JT-60U experiments, the frequency could be identified in real time using a fast Fourier transform [22] because the mode frequency was quite uniform and changed only slowly, with a typical timescale of several hundred milliseconds. If the mode oscillations are irregular, such a modulation scheme becomes difficult, and another scheme may need to be developed. Furthermore, as shown in Fig. 12, a collapse-induced NTM was triggered even during feedback control of the beta value (~pressure). This indicates that feedback control of profiles is important to avoid such a collapse when operating close to the mode onset regime.

This analysis revealed that in around 80% of the analyzed discharges, a 2/1 mode is triggered without a large MHD event. In some of the discharges, the NTM onset time appears to coincide with an ELM crash time, which suggests that an ELM is one of the candidates for NTM onset. Even so, the effect of ELMs on NTM growth is small (this can also be seen in Fig. 1, where some ELMs appear during regular oscillations, but the mode amplitude is almost unaffected). In some discharges, as shown in Fig. 1, NTMs do appear and grow between ELMs, which indicates there is another cause for the onset. The reason for the onset for such cases has not been clarified and remains as a future study.

Acknowledgments

This study was partially supported by a Grant-in-Aid for Young Scientists (B) #22760662 from MEXT Japan.

[1] T.C. Hender, J.C. Wesley, J. Bialek *et al.*, Nucl. Fusion **47**, S128 (2007).
[2] H. Zohm, G. Gantenbein, G. Giruzzi *et al.*, Nucl. Fusion **39**, 577 (1999).
[3] G. Gantenbein, H. Zohm, G. Giruzzi *et al.*, Phys. Rev. Lett. **85**, 1242 (2000).
[4] M. Maraschek, G. Gantenbein, Q. Yu *et al.*, Phys. Rev. Lett. **98**, 025005 (2007).
[5] R.J. La Haye, S. Günter, D.A. Humphreys *et al.*, Phys. Plasmas **9**, 2051 (2002).
[6] C.C. Petty, R.J. La Haye, T.C. Luce *et al.*, Nucl. Fusion **44**, 243 (2004).
[7] R. Prater, R.J. La Haye, T.C. Luce *et al.*, Nucl. Fusion **47**, 371 (2007).
[8] A. Isayama, Y. Kamada, S. Ide *et al.*, Plasma Phys. Control. Fusion **42**, L37 (2000).
[9] A. Isayama, Y. Kamada, N. Hayashi *et al.*, Nucl. Fusion **43**, 1272 (2003).
[10] A. Isayama, N. Oyama, H. Urano *et al.*, Nucl. Fusion **47**, 773 (2007).
[11] A. Isayama, G. Matsunaga, T. Kobayashi *et al.*, Nucl. Fusion **49**, 055006 (2009).
[12] N. Hayashi, A. Isayama, K. Nagasaki *et al.*, J. Plasma Fusion Res. **80**, 605 (2004).
[13] K. Nagasaki, A. Isayama, N. Hayashi *et al.*, Nucl. Fusion **45**, 1608 (2005).
[14] L. Urso, H. Zohm, A. Isayama *et al.*, Nucl. Fusion **50**, 025010 (2010).
[15] F.L. Waelbroeck, Nucl. Fusion **49**, 104025 (2009).
[16] O. Sauter, R.J. La Haye, Z. Chang *et al.*, Phys. Plasmas **4**, 1654 (1997).
[17] A. Gude, S. Günter, S. Sesnic *et al.*, Nucl. Fusion **39**, 127 (1999).
[18] A. Isayama, Y. Kamada, T. Ozeki *et al.*, Nucl. Fusion **41**, 761 (2001).
[19] M. Shimada, D.J. Campbell, V. Mukhovatov *et al.*, Nucl. Fusion **47**, S1 (2007).
[20] A. Isayama, G. Matsunaga, Y. Ishii *et al.*, Plasma Fusion Res. **5**, 037 (2010).
[21] S. Takeji, Y. Kamada, T. Ozeki *et al.*, Phys. Plasmas **4**, 4283 (1997).
[22] T. Kobayashi, M. Terakado, F. Sato *et al.*, Plasma Fusion Res. **4**, 037 (2009).